Silicon (2023) 15:7157–7170
https://doi.org/10.1007/s12633-023-02527-y

RESEARCH

Physico-Mechanical and Microstructure Characteristics of Porous Mullite Ceramics

Amira M. EL-Rafei[1] · **T. S. Mansour**[1]

Received: 25 February 2023 / Accepted: 19 May 2023 / Published online: 27 June 2023

Abstract
Porous mullite ceramics were prepared from mixtures of Egyptian kaolinite-clay and calcined α-alumina powder. The effects of two methods of compaction as well as two types of binder were investigated. The influence of sintering temperature on the physical properties, crystalline phase, compressive strength and microstructure was studied. Mullite bodies processed by uniaxial pressing utilizing 15wt. % water at 1500°C for 2h exhibited the highest compressive strength of 150 MPa and bulk density of 2.1 g/cm^3, as well as, an open porosity of 35%. In the present study, the only stoichiometric mullite was achieved by the crystallization of metakaolin. The mullite crystallizing out from the liquid phase was rich in silica, as determined by EDS, while that resulting from alumina grains was rich in alumina. The microstructure showed that primary mullite appeared at 1200°C, beside the unreacted alumina particles. On the other hand, at 1400°C alumina particles started to react with the glassy phase to form parallel laminates of mullite.

Keywords Kaolinite · Mullite · Alumina · Porous materials · Cristobalite · Microstructure

1 Introduction

Ceramic membranes have excellent strength, good corrosion resistance, high chemical and thermal stability, good anti-fouling properties and long life requirements to operate at high temperature, highly corrosive and high-pressure filtration environment, compared to those prepared from polymers. However, the workability of these membranes and the cost of production restrict their application. The utilization of cheaper raw materials may reduce the cost of production of these membranes [1].

Mullite ($3Al_2O_3{\cdot}2SiO_2$) is a potential candidate for porous ceramic membranes with high strength and creep resistance, a low thermal expansion coefficient, and proper chemical and thermal stability. Porous mullite ceramic membranes have been significantly applied in the fields of catalyst carriers, filters and ceramic supports for filtration membranes [2].

There are several methods for the synthesis of mullite ceramics, including reaction sintering, spark plasma and microwave-assisted sintering, gel casting, foaming and freeze-drying, where it is supplied in the form of powder or dense or porous bodies.

Researchers concentrate on the simplicity of preparation methods and low-cost raw materials, such as the use of solid wastes to replace industrial raw materials, and using pressure-less sintering in an ambient atmosphere [3].

High alumina kaolin and coal fly ash are adequate mix for the synthesis of low-cost mullite ceramics [4]. Usually pure alumina or its precursors are added to satisfy the mullite composition.

In general, the gradual dissociation of kaolin with temperature gives first meta-kaolinite, which has a spinel structure, and readily transforms into mullite (the primary form) beside amorphous silica at around 980°C.

As the temperature increases, the amount and size of mullite crystals increase, leaving behind excess silica as a glassy phase or free amorphous silica in the matrix [1].

Several studies demonstrated that primary mullite transformed into secondary mullite in the presence of an amorphous alkali-rich glass [5–11].

Schuller [10] described two different types of mullite of different morphologies from studies of porcelain and he showed that primary mullite transforms into secondary mullite at 1400°C and because of the complete dissolution of quartz, a texture consisting of glass and mullite needles results.

✉ Amira M. EL-Rafei
am.amin@nrc.sci.eg

[1] Refractories, Ceramics and Building Materials Department, National Research Centre, 33 El Buhouth St., Dokki, Cairo 12622, Egypt

Some studies explained that primary mullite is formed in areas rich in clay, while secondary mullite is formed in areas containing impurities such as potassium, which acts as flux to assist the formation of the liquid phase, allowing the crystallization of longer secondary mullite crystals [12, 13].

However, some studies have shown that an external alumina source reacts with the excess SiO_2 from clay to form secondary mullite over a wide temperature range [1–3, 14–16].

Chen et. al. [14] prepared mullite by reactive sintering of a mixture of kaolin combined with $Al(OH)_3$ and AlF_3 as alumina sources to obtain macroporous mullite. Whereas, porous mullite with an interlocked needle-shaped microstructure was synthesized from China clay and aluminium fluoride trihydrate ($AlF_3{\cdot}3H_2O$), as reported by Rashad and Balasubramanian [1]. Also, bauxite and kaolin powders were used as precursors to prepare porous mullite ceramic membranes by Zhu et.al. [2].

In some cases, kaolin clay was used for the preparation of mullite membranes and the remaining free silica was removed from the sintered membrane by a strong alkali solution (20 wt.% NaOH) in an oven at 80°C for 5 h to achieve higher porosity [17].

When kyanite was added to kaolin, bauxite and feldspar to prepare porous mullite, it enhanced both the porosity and thermal stability by lowering the temperature of glass formation and promoting crystallization of mullite [18].

Hou et. al. [19] have studied the effect of MoO_3 on mullite bodies prepared from kaolin and Al_2O_3. They showed that MoO_3 addition lowered the secondary mullitization temperature to below 950°C. They reported that the added Al_2O_3 powders dissolved in the silica-rich liquid phase to form the secondary mullite, where the crystal growth was controlled by diffusion. Therefore, the rate-determining step for crystal growth is the dissolution velocity of alumina into the silica-rich liquid phase.

Hou and Cui et. al. [20] studied the impact of specific sintering additives; TiO_2, MgO and MoO_3 on mullite bodies, prepared from kaolin and Al_2O_3. They confirmed that the mullite transformation temperature was strongly affected by the type of sintering additives, as they lower the melting point of silicon-rich liquid. The addition of MgO and MoO_3 promoted the formation of secondary mullite with a needle-like morphology. However, the addition of TiO_2 retarded the mullite formation, as it participated in the formation of aluminum titanate or entered the mullite structure.

Sainz et. al. [15] investigated the microstructure of mullite prepared through the sintering reaction of kaolinite-alumina mixtures. They showed the existence of a bimodal mullite morphology, corresponding to primary (elongated columnar grains) and secondary (equiaxed grains) forms.

Whereas, porous support with 96 wt.% mullite and 65 % open porosity was developed at a relatively lower temperature of 1300°C from clay and aluminium fluoride trihydrate mixture by adding 10 wt.% alumina into this mixture. The addition of alumina enhanced the mullite formation by consuming the excess SiO_2 in the matrix [16].

The objective of this work is to fabricate porous mullite ceramics from cheaper local raw Egyptian kaolin-clay materials by adding calcined alumina.

The effect of the addition of various amounts of either water or PVA on the degree of compaction of the particles and the form of processing on sintering and physico-mechanical properties, as well as the microstructure of the prepared mullite bodies, is investigated.

2 Materials and Experimental Procedure

2.1 Preparation of Mullite Bodies

The following raw materials were supplied by Middle East Mining Company (Memco) and Alexandria Company for Refractories (ACR) imported calcined alumina from Alcoa; refined local Egyptian kaolin-clay (with grain size ranging from 0.7 to 1 μm); and α-Al_2O_3 (purity 99.5%, with grain size ranging from 6 to 7 μm), respectively. The kaolin-clay was not calcined, as preferred by many authors, to make use of the plasticity of the kaolin-clay in the forming process. The ratios corresponding to the stoichiometric composition of mullite, ($3Al_2O_3{\cdot}2SiO_2$), were weighted, mixed and ball-milled for 12 h using a polyethylene bottle with alumina balls. The powder was mixed by using two binders, namely, tape water and polyvinyl alcohol, PVA, $[CH_2CH(OH)]_n$, with different ratios (5, 10, 15 and 20%). Then processed in the form of pellets of 25 mm in diameter and 15–16 mm in thickness, applying two different shaping methods, i.e., uniaxial pressing at 30 MPa and hand pressing.

The two main batches obtained were designated as W and P, with Nos. 1 and 2 referring to the water and PVA and the processing method. i.e., W1 and P1 were uniaxially pressed at 30 MPa, while W2 and P2 were hand pressed. Moreover, each subgroup was divided into four groups according to the ratio of added water or PVA. The batches were briefly named, as summarized in Table 1. Such as the sample with 10 wt.% of water and uniaxially pressed was designated WP10, while the sample with 15 wt.% of PVA and hand pressed was designated PH15.

Table 1 List of prepared samples with different methods

		5%	10%	15%	20%
Uniaxial Pressing	Water	WP5	WP10	WP15	.....
	PVA	PP5	PP10	PP15	.....
Hand Pressing	Water	WH5	WH5	WH15	WH20
	PVA	PH5	PH10	PH15	PH20

Table 2 The chemical composition of local Egyptian kaolin

Constituent	%
SiO_2	47.533
Al_2O_3	36.986
TiO_2	1.334
Fe_2O_3	0.405
CaO	0.291
MgO	0.054
K_2O	0.044
Na_2O	0.092
P_2O_5	0.739
SO_3	0.365
SrO	0.408
Total traces	0.349
Loss of ignition	11.400

The processed samples were left to dry for 48 h at room temperature, and then fired for 2 h in an ambient atmosphere in a muffle furnace at the given temperatures; 1150, 1300, 1400, 1500 and 1550°C with a heating/cooling rate of 5°C/min. The samples prepared by uniaxial pressing utilizing 20 wt% water or PVA failed to keep their shapes.

2.2 Characterization

The starting materials were quantitatively analyzed by wavelength dispersive X-ray fluorescence (AXIOS, WD-XRF Sequential Spectrometer, (Panalytical, 2005). The results obtained are shown in Table 2. The particle size of the kaolin and calcined alumina powders was measured by Dynamic Light Scattering (DLS) (Malvern Zeta Sizer Instrument ZS-Nano, UK, λ=532 nm) at a temperature of 25°C. The powder samples were dispersed in ethanol and sonicated before measurement.

The X-ray powder diffraction (XRD) patterns of samples were carried out on a Rigaku D/Max-3c X-ray diffractometer utilizing a CuKα radiation and operated at 40 kV and 50 mA.

The bulk density and open porosity were measured for all samples by Archimedes' method. The linear change of the samples at different temperatures was calculated by linear change (%) = [(E − E′)/E] × 100, where E refers to the diameter of the sample before firing, while E′ refers to the sample diameter after firing at elevated temperatures. The compressive strength was measured for all samples by (Matest 24030 Brembate Sopra – Italy, which has a maximum load capacity of 2000 KN. The test samples are in pellets

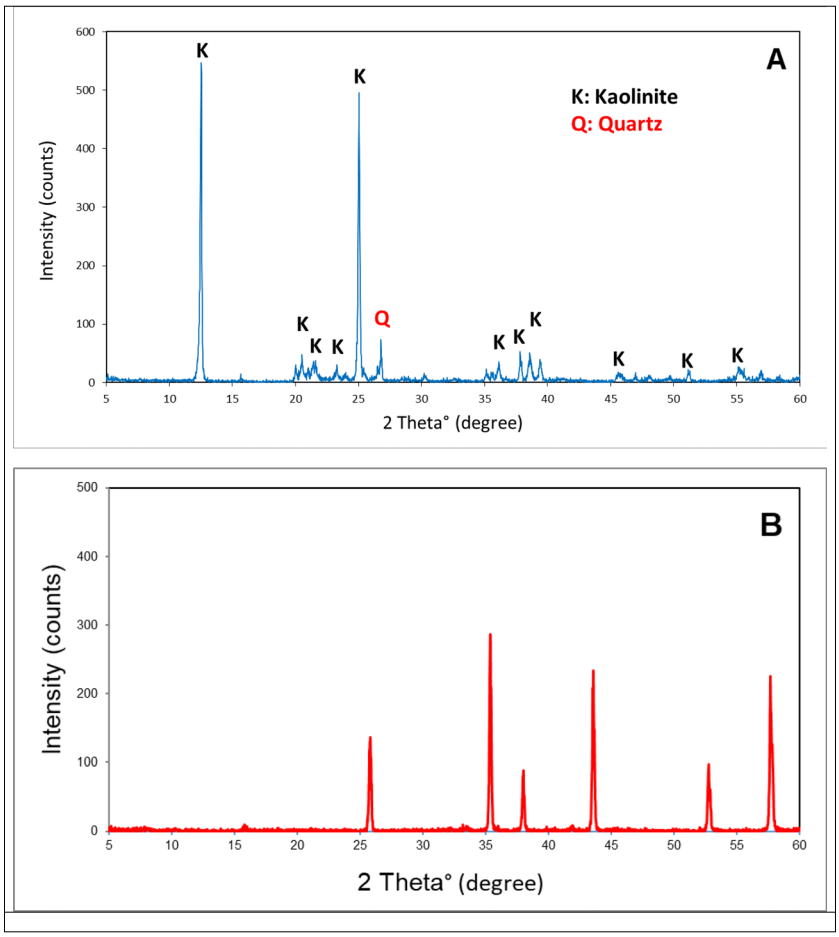

Fig. 1 XRD patterns of (**A**) kaolin-clay and (**B**) calcined alumina

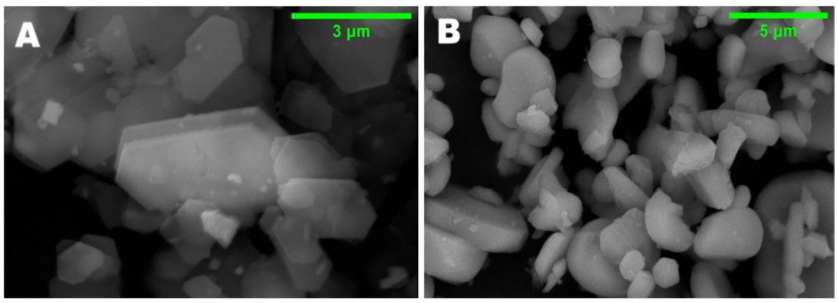

Fig. 2 FE-SEM images of the **A**) kaolin clay and **B**) α-alumina

form with a 25 mm diameter; in all tests, the average values of five samples are estimated.

The microstructure of the fractured surfaces of the selected samples was examined under scanning electron microscopy (QUANTA FEG, 250, Netherlands) after coating with a thin film of gold**.**

3 Results and Discussion

3.1 Characterization of the Raw Materials

The chemical composition (XRF) of Egyptian kaolin-clay is shown in Table 2. The ignition loss of kaolin was 11.40 wt.%. The main constituents were alumina (36.98 wt.%, silica (47.53 wt.%) and the rest were impurities. The main phases detected by XRD were kaolinite as the major phase and quartz as a minor phase, whereas α-alumina was the sole phase detected by XRD, as shown in Fig. 1A and B.

The morphology of the kaolinite-clay and alumina particles is shown in Fig. 2. The kaolinite-clay particles were flaky in shape. Some large kaolin flakes were stacked together to form agglomerates (Fig. 2A). The crystals exhibited a hexagonal structure (Fig. 2B). Alumina crystals showed a crystal size range of 0.5-2 µm (Fig. 2B).

The particle size and size distribution of kaolinite-clay and calcined alumina are shown in Fig. 3. The kaolin presented a median diameter of 0.77 µm On the other hand; the calcined alumina exhibited an average diameter of 0.55 µm.

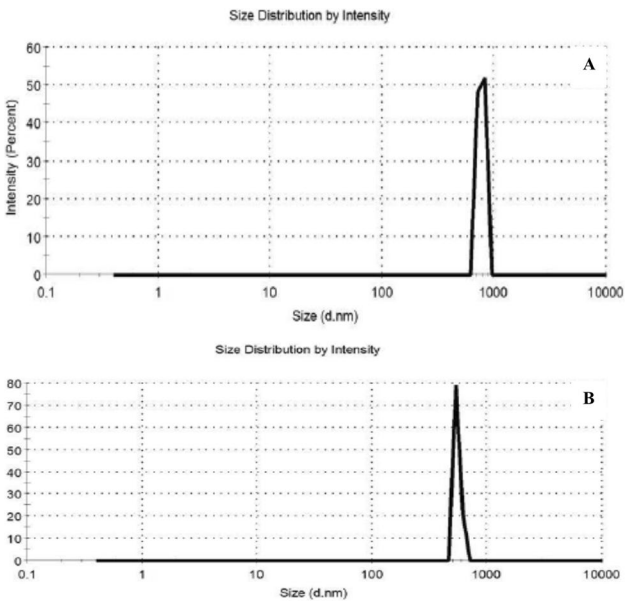

Fig. 3 The particle size distribution for (**A**) local kaolin clay and (**B**) calcined alumina

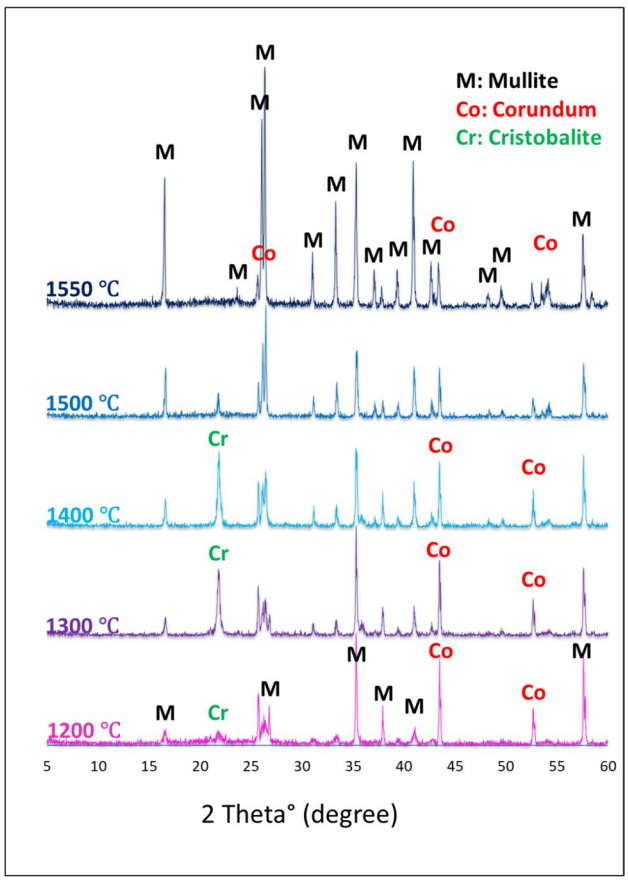

Fig. 4 XRD patterns of fired mullite bodies at different firing temperatures

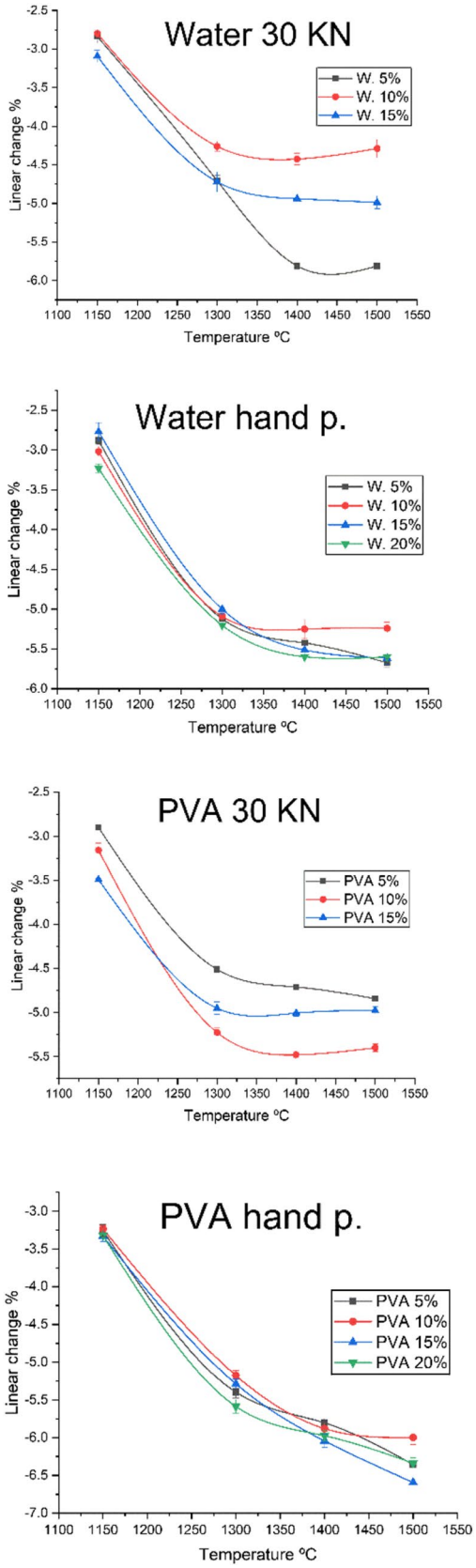

Fig. 5 The linear change % versus temperature for mullite bodies

3.2 Characteristics of the Fired Mullite Bodies

3.2.1 Phase Composition

The X-ray diffraction patterns of mullite bodies fired for two hours at temperatures between 1200 and 1550°C are shown in Fig. 4. The sample sintered at 1200°C contains mullite ($3Al_2O_3{\cdot}2SiO_2$, orthorhombic, PDF#15-0776) and corundum (Al_2O_3, hexagonal, PDF#10-0173) beside Cristobalite (SiO_2, tetragonal, PDF#39-1425). These results are in accordance with those found by Deutou et al. [18]. The dissociation of kaolin to give mullite and amorphous silica followed the Eqs. (1 and 2):

$$Al_2O_3.2SiO_2.2H_2O \xrightarrow{\text{Heating}} Al_2O_3.2SiO_2 + 2H_2O \quad (1)$$

$$3\left(Al_2O_3.2SiO_2\right) \longrightarrow 3Al_2O_3.2SiO_2(\text{primary mullite}) + 4\,SiO_2(\text{at } 1200°C) \quad (2)$$

where the free amorphous silica crystallizes later into Ill-cristobalite. XRD intensities of both mullite and cristobalite

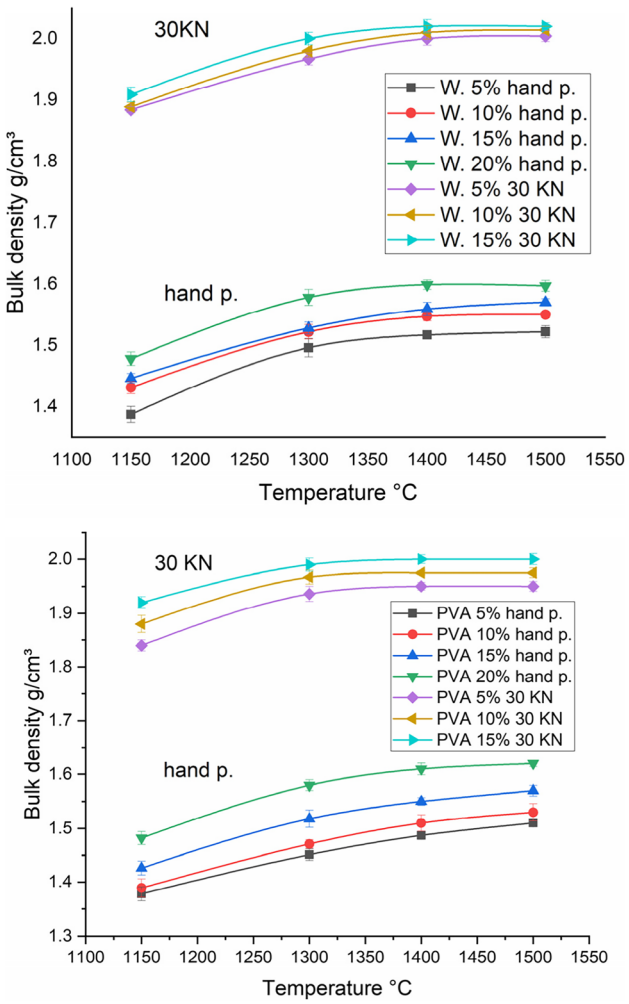

Fig. 6 Bulk density versus temperature for mullite bodies

phases are more pronounced at higher temperatures, from 1300 to 1400°C, which indicates that the mullitization reaction is proceeding. Most of the corundum did not participate in the reaction with cristobalite to form mullite in this temperature range. Whereas, increasing the sintering temperature to 1500°C showed that the peaks of cristobalite had lessened, indicating its reaction with alumina to form mullite, while part of the cristobalite was consumed in the glassy phase formation. The reaction can be illustrated by the Eq. (3)

$$3Al_2O_3 + 2SiO_2 \longrightarrow 3Al_2O_3.2SiO_2 \quad (3)$$

Between 1500 and 1550°C, the cristobalite diffraction peaks had completely vanished and the intensity of the mullite peaks was more pronounced. Still, relics of corundum were recorded as a minor phase. Back in mind, the added calcined alumina and kaolin were in the ratio corresponding to the nominal chemical composition of mullite. This may be attributed to the fact that part of the cristobalite was consumed in the formation of the glassy phase. Accordingly, the mullitization reaction is nearly complete at 1550°C. Several authors [16, 21–27] have reached the same conclusion and reported that the sintering temperature is between 1500 and 1600°C for the complete mullitization reaction.

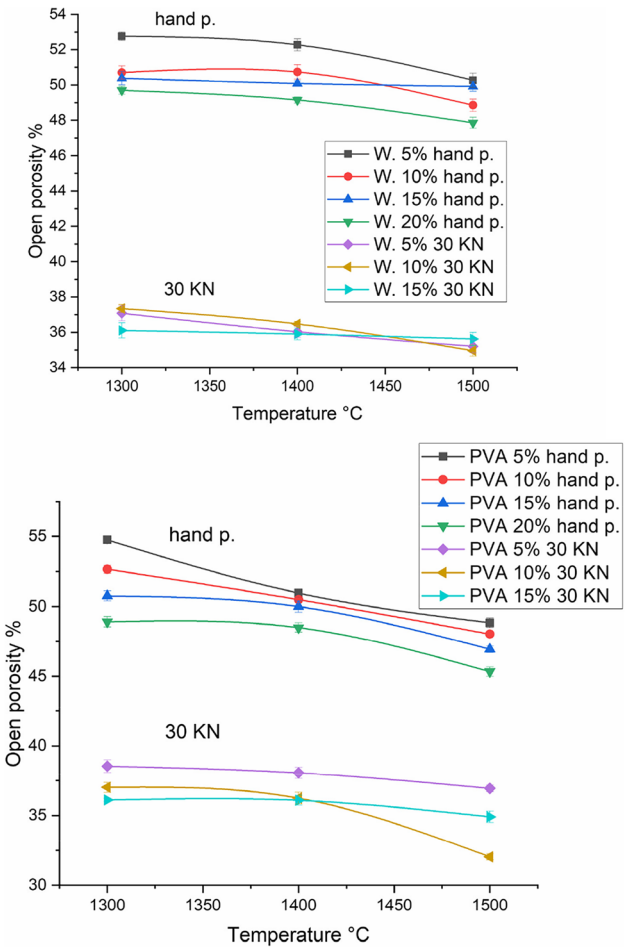

Fig. 7 The open porosity % versus temperature for mullite bodies

3.2.2 Physical Properties of the Formed Mullite Bodies

The results of the physical properties in terms of the change in dimensions of the fired bodies, bulk density and open porosity of the fired ones are affected by the processing mode, sintering temperature and type of plasticizer used. As anticipated, the type and amount of the plasticizer played a conspicuous role in these properties.

The results of the linear change of the fired bodies are demonstrated in Fig. 5. It displays the dimensions shrinkage percent of the bodies at temperatures ranging from 1150 to 1500℃. Shrinkage increases with increasing sintering temperature up to 1400℃, as the densification process is dominant below 1400°C and therefore the shrinkage percent increases with increasing temperature. Thereafter, the recorded shrinkage is almost negligible above 1400°C. This steady state can be attributed to the two adverse reactions simultaneously taking place: first, a decrease in density. Due to the mullite formed, which induces volume expansion and has less density than the alumina precursor, and second, the shrinkage accompanying the sintering process; these two reactions nullify each other. In general, the hand-pressed samples showed a shrinkage percentage larger than the uniaxially pressed ones. The maximum shrinkage was recorded for the hand-pressed bodies processed using PVA.

Figure 6 shows the change in the bulk density of the fired bodies. Sintering was more pronounced at low temperatures range than in the higher ones (1400 to 1500℃).

This might be due to several parameters that affect the bulk density, such as the formation of mullite (theoretical density of 3.17 g/cm^3) at the expense of alumina (theoretical density of 3.99 g/cm^3) and the mullitization reaction, which is associated with volume expansion.

It is noted that the samples processed by uniaxial pressing showed higher values of bulk density than samples processed by hand pressing; moreover, the uniaxially pressed samples processed with water showed the highest bulk density value.

The recorded range of bulk density at the firing temperature of 1150 to 1500℃ for the uniaxially pressed samples (subgroups W1 and P1) lies between 1.84 and 2.03 g/cm^3, whereas the hand pressed samples range between 1.35 and 1.63 g/cm^3 (subgroups W2 and P2).

The results of the open porosity of the samples sintered between 1300 and 1500℃ decrease over the total firing range, as shown in Fig. 7. The uniaxially pressed samples (subgroups W1 and P1) show lower values (between 35 and 40 %), whereas the hand-pressed ones (between 50 and 55 %), (subgroups W2 and P2). Meanwhile, at 1500℃, the maximum open porosity (~ 55%) was attained for PH5 samples.

The above results demonstrated that the type and amount of the plasticizer, pressing mode, and sintering temperature affected the final product properties and, accordingly, will affect their applications.

3.2.3 Microstructure of the Fired Bodies

Effect of Temperature on the Microstructure of Sintered Samples The effect of sintering temperature between 1200 and 1500°C on the microstructural changes of the uniaxially pressed samples processed using 5 wt. % water, as an example, is demonstrated in Fig. 8.

The matrix of the sample fired at 1200°C is formed of primary nanometric mullite crystals (Fig. 8 A), preserving the hexagonal platy shape of the original structure of the kaolinite mineral [12, 28], leaving behind the unreacted α-alumina and cristobalite grains (Fig. 8 A and B). In this case, the formation of mullite took place via the solid state reaction of kaolin.

As the temperature increases to 1300°C, two biomodal characteristic regions appear; one corresponding to the columnar primary mullite crystals, which increase in size compared to mullite crystals at 1200°C, and the other is the unreacted region of α-alumina grains with varying sizes, (Fig. 8 C and D), giving a porous network. There is no evidence of the presence of the glassy phase at 1300°C.

As the temperature increased to 1400°C (Figs. 8 E and F), three distinct polymorphs of mullite crystals were spotted: columnar primary, secondary acircular and platy-like mullite phases. the former columnar mullite, originating from kaolin, that grew in size, occurring in agglomerates; secondary mullite, resulting from the dissolution of the primary mullite phase in the glassy phase, giving acircular shaped crystals; and finally, the platy-like mullite, formed by the

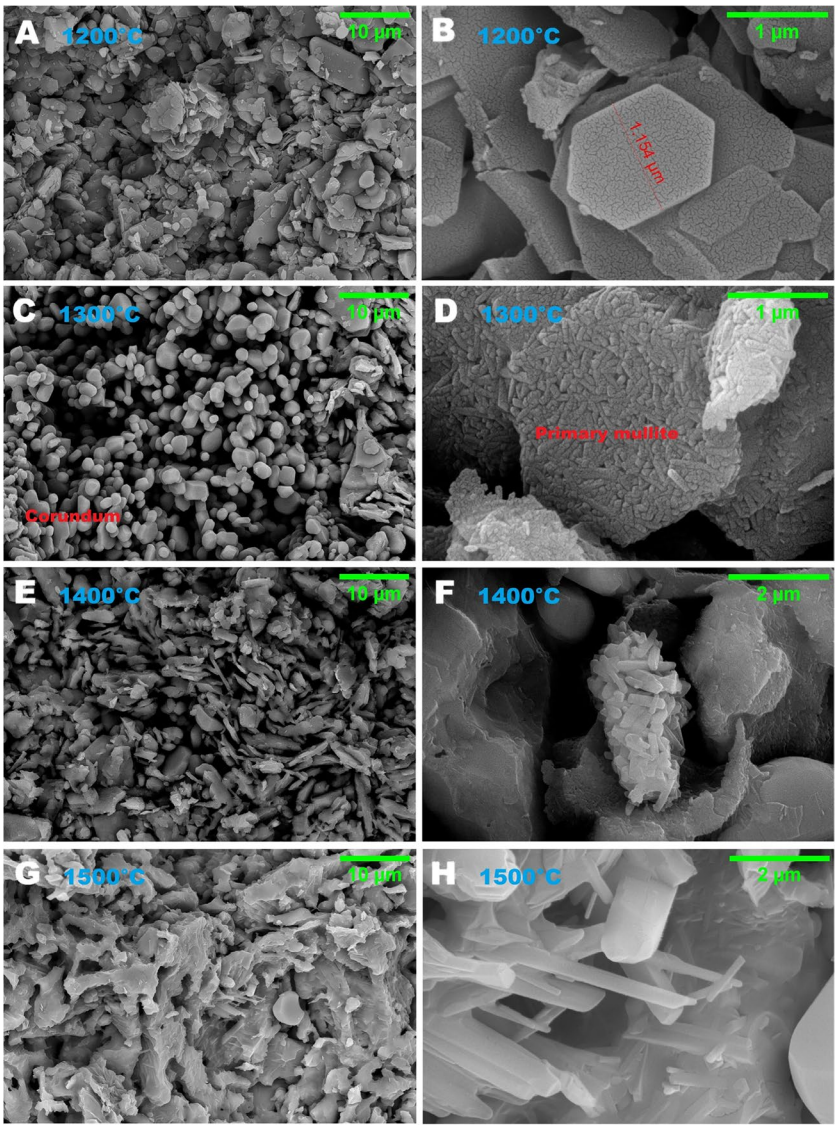

Fig. 8 FE-SEM micrographs of fired uniaxial pressed samples with 5 wt.% water sintered for 2 h at different temperature at, **A**) 1200, **C**) 1300, **E**), 1400 and **G**) 1500°C. (**B, D, F**, and **H**) images at higher magnification

dissolution-diffusion reaction of alumina and silica. This indicates that α-alumina grains started to react with the siliceous glassy phase to form mullite. Thereby, they lose their original shape. So mullite appeared as platy-like shaped crystals sticking together, forming a bundle of laminated crystals adhering to the relics of alumina grains (Fig. 8 F). These results are consistent with XRD results, where the intensities of the α-alumina peaks started to decrease at 1400°C.

At 1500°C, the resulting microstructure appeared more compact with less pore volume (Fig. 8 G). Meanwhile, the aspect ratio of the acircular mullite increases (crystals >5 μm) forming an interlocked structure (Fig. 8 H).

It could be concluded that the fracture behavior of the samples fired at 1200 and 1300°C is mainly transgranular, as there is no glassy phase in those samples, whereas the samples fired at 1400 and 1500°C show mainly an intergranular fracture due to the presence of the glassy phase, as the glassy phase could bond the mullite crystals together enough to undergo the intergranular fracture.

EDS analysis of the different phases formed is shown in Fig. 9. It is worth mentioning that there are two different compositions detected for columnar primary mullite, one satisfying the mullite formula ($3Al_2O_3.2SiO_2$) (Fig. 9 A), while the other is slightly higher in silica content (Fig. 9 B).

The secondary mullite that crystallized out of the glassy phase was richer in silica than the primary mullite (Fig. 9 C). The same result was reached by Lee et.al. [13]. They demonstrated that the chemical composition of primary mullite is rich in alumina, while that of secondary mullite is rich in silica.

On the other hand, for the platy-like crystal mullite, EDS revealed that its composition was higher in alumina, as expected (Fig. 9D). The EDS of unreacted alumina grains was also shown in Fig. 9E.

Effect of Processing Parameters The microstructure of the PP5 and PP15 groups and WP5 and WP15 groups sintered for 2 hours at 1500°C is shown in Figs. 10 and 11,

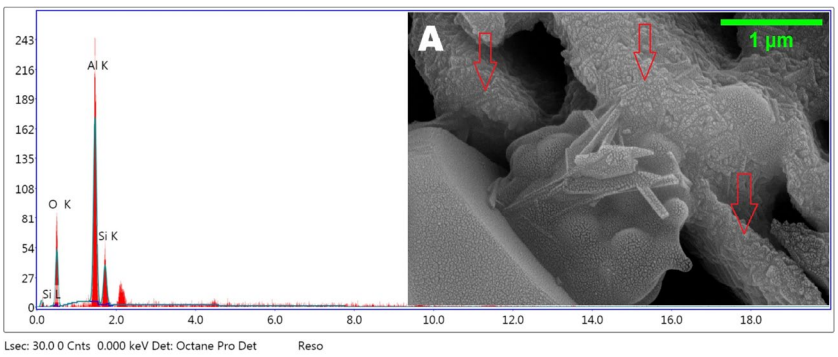

Element	Weight %	Atomic %	Net Int.	Error %
O K	40.55	53.75	26.24	12.68
AlK	43.92	34.52	104.91	5.53
SiK	15.53	11.73	23.78	12.73

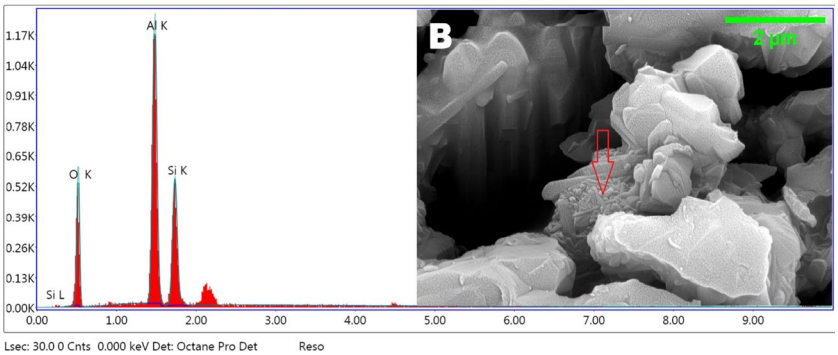

Element	Weight %	Atomic %	Net Int.	Error %
AlK	30.96	23.23	269.35	4.81
SiK	19.4	13.98	128.91	7.28
Oxygen	49.64	62.8	0	0

Fig. 9 EDs spot analysis of the red arrow

Fig. 9 (continued)

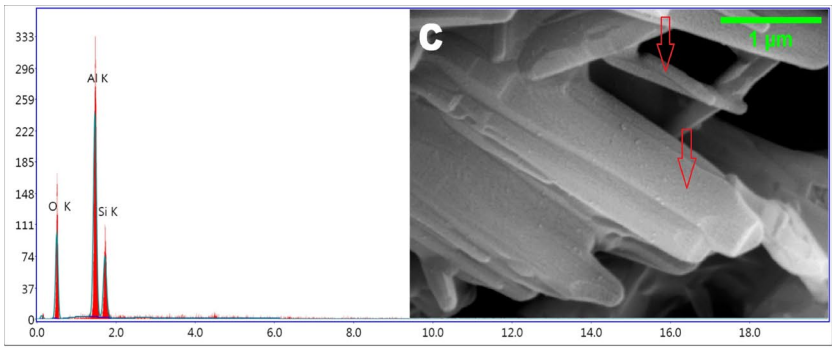

Element	Weight %	Atomic %	Net Int.	Error %
O K	44.98	58.26	51.71	10.57
AlK	37.77	29.01	149.16	5.23
SiK	17.26	12.73	47.4	9.68

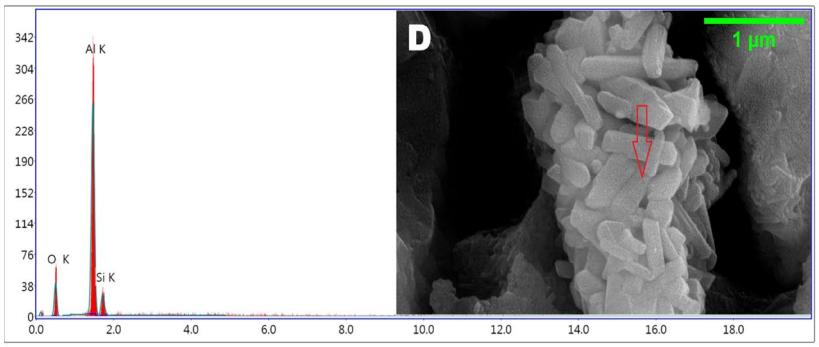

Element	Weight %	Atomic %	Net Int.	Error %
O K	31.78	44.16	21.2	13.41
AlK	57.13	47.07	161.12	4.55
SiK	11.09	8.77	16.94	14.04

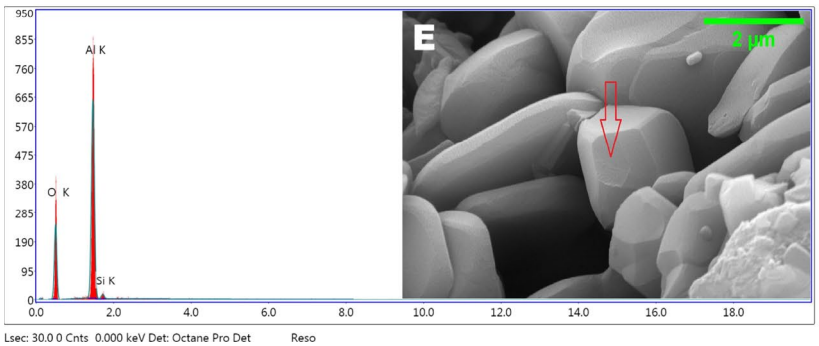

Element	Weight %	Atomic %	Net Int.	Error %
O K	47.97	60.9	126.07	8.86
AlK	50.05	37.68	403.76	4.57
SiK	1.97	1.43	9.72	20.56

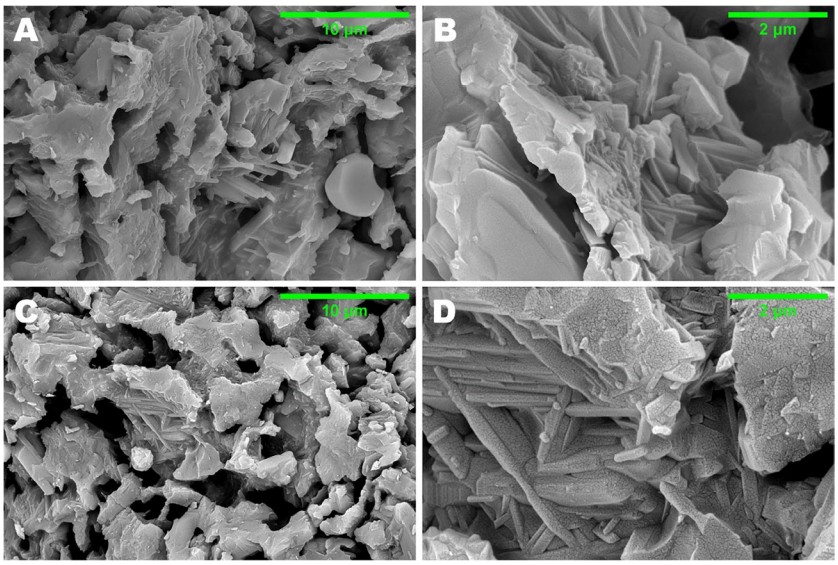

Fig. 10 FE-SEM micrographs of samples sintered for 2 h at 1500°C, **A**) PP5 and **C**) PP15 %, (**B** and **D**) at high magnification.

respectively. The microstructure of all samples was marked by columnar primary mullite along with acircular mullite, which is embedded in a glassy matrix (as shown in Figs. 10A-D and 11A-D), besides unreacted alumina grains.

The acircular mullite shows an interlocked structure, which remarkably improved the interconnection of pores (Figs. 10A, 11B and C).

The microstructure of the PH5 and PH20 groups and WH5 and WH20 groups sintered for 2 hours at 1500°C is shown in Figs. 12 and 13, respectively.

The general trend for the samples processed using PVA was characterized by large voids as PVA is a large molecule (Fig. 12A-D), while the microstructure of the samples processed using water was characterized by an interconnected porous structure. In addition, the distribution of pores when water was used was more homogenous (Fig. 13A-D).

Also, the samples processed by uniaxial pressing show a more dense structure than those processed by hand pressing with a given amount of either water or PVA, which is consistent with the bulk density results (see Fig. 6). In summary, the effect of using the uniaxial pressing and water as binder on the densification is more pronounced than the hand pressing and PVA as binder, which corresponds to the good green body packaging.

3.2.4 Mechanical Properties of the Prepared Samples

The compressive strength of the sintered mullite samples at different temperatures is shown in Fig. 14. The main criteria that influence the compressive strength are the type of phases developed, grain size, presence of the glassy

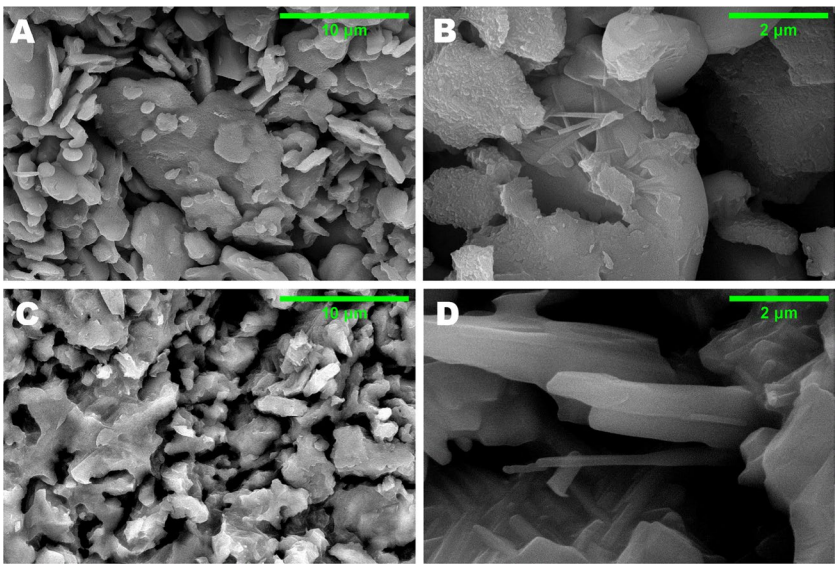

Fig. 11 FE-SEM images of samples sintered for 2 h at 1500°C. **A**) WP5 and **C**) WP15, (**B** and **D**) at high magnification.

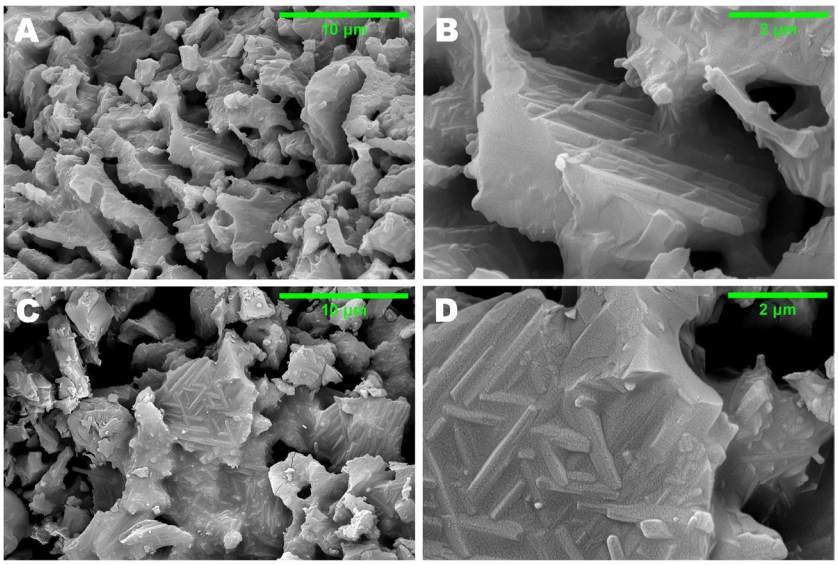

Fig. 12 FE-SEM micrographs of samples sintered for 2 h at 1500°C. **A**) PH5 and **C**) PH20, (**B,D**) at higher magnification

phase and porosity [29]. The values of the compressive strength increased for all batches over the firing temperatures from 1300 to 1500°C. The size and shape of the crystalline phases developed might have played an important role as these crystalline phases form a mesh [19, 20, 30]. As a result of the increase in aspect ratio of the acircular mullite formed, which forms an interlocked structure, i.e., the microstructure developed is responsible for the figures obtained.

For the WP5 and WP15 batches, the bulk density is maximum, so the expected compressive strength is maximum (154 MPa), as confirmed in Fig. 14. On the other hand, the batches PH5 with a minimum value of bulk density showed a minimum compressive strength of 7.6 MPa.

3.2.5 Mechanism of Mullite Formation

In the kaolinite-alumina mixture, several studies reported that the mechanism of the crystallization of primary mullite from metakaolinite [20, 31, 32] occurs around 1000°C by instantaneous mullite nucleation after the dehydroxylation of kaolinite reaction. It is accelerated by the almost ideal molecular mixing of alumina and silica polyhedra in the structure. i.e., mullite nucleates by short range diffusion [33]. Through the phase boundary, the mullite crystallizes out, attaining a preferred orientation with the c axis parallel to <110> of the Al–Si spinel phase and metakaolinite. The Al–Si spinel phase caused the collapse of the metakaolinite structure, whereas the growth of the mullite

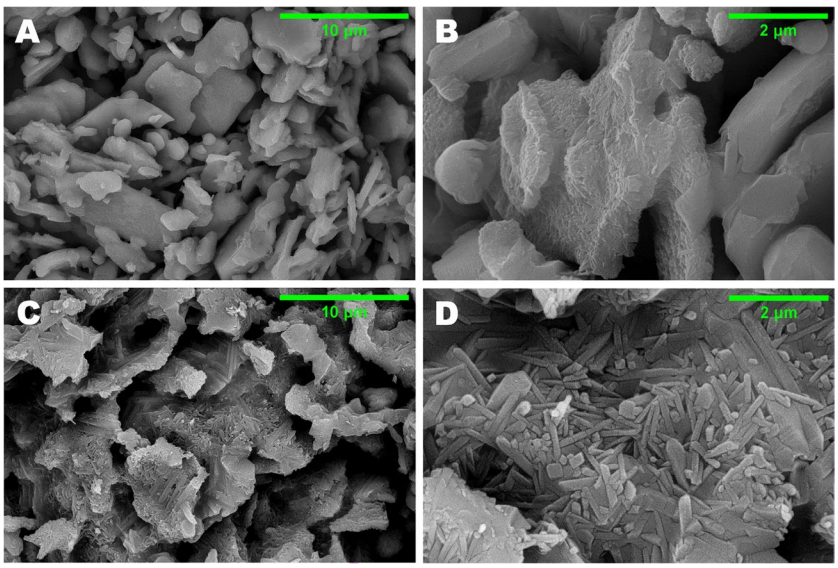

Fig. 13 FE-SEM micrographs of samples sintered for 2 h at 1500°C. **A**) WH5 and **C**) WH20, (**B,D**) at higher magnification

crystals is accelerated by an instantaneous nucleation process through short distance diffusion, thereby preserving the original platy morphology of the kaolin [34].

While the secondary mullite crystallization took place through the dissolution of the primary mullite phase in the glassy phase, giving acircular shaped crystals [35].

While the mullite formed by the diffusion reaction of the siliceous liquid phase into the alumina grains gave platy mullite by the mechanism termed dissolution-diffusion, in some studies this mullite is called tertiary mullite [36].

Tarvornpanich [37] reported that kaolin clay fired for 3 h at 1200°C contained scaly primary and rod-like ~1–2μm long secondary mullite. He explained the formation of primary mullite in the area once rich in clay and the formation of rod-like mullite in the area containing impurities, which act as flux to facilitate the liquid formation on firing, allowing the crystallization of longer crystals. In another study, Percival et. al. [38] declared that, in

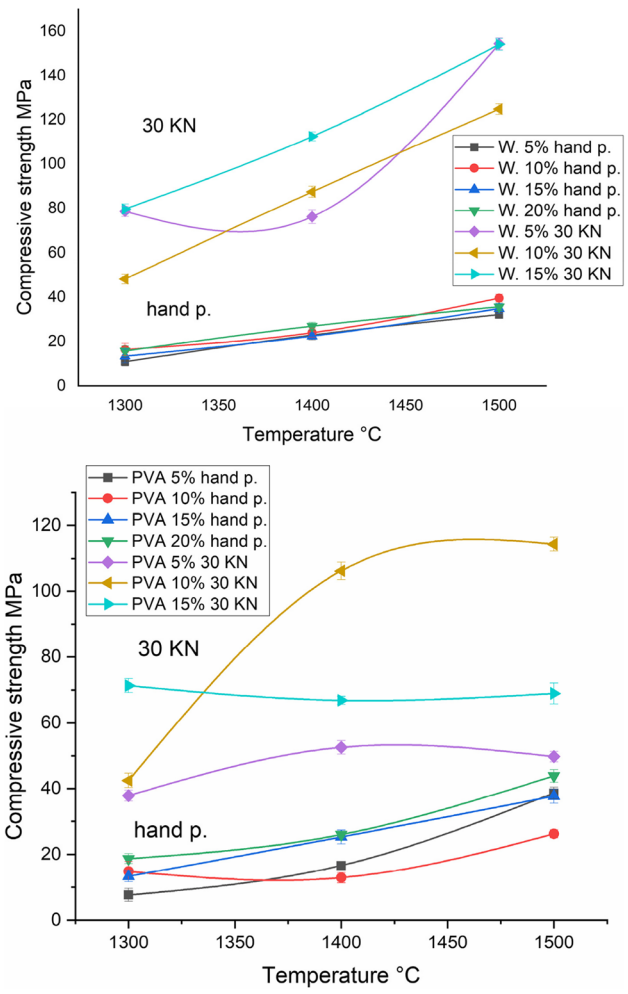

Fig. 14 The compressive strength versus temperature for mullite bodies

kaolinite at 950°C, the metakaolinite is completely decomposed. The resulting spinel-type phase, which is associated with amorphous SiO_2 and some poorly crystalline "primary" mullite, is ɣ-Al_2O_3 (crystalline) rather than an Al-Si spinel. At >1100 °C, secondary mullite therefore forms primarily from the ɣ-Al_2O_3/amorphous SiO_2 reaction and the recrystallization of primary mullite, whereas excess amorphous SiO_2 eventually crystallizes as cristobalite.

Aza et. al. [12] stated that the formation of primary mullite, side by side with a cubic phase, Si-Al spinel, and an amorphous silica-rich phase, was reached at ~980–992°C. From~1136°C growth of mullite crystals occurs, and at T > ~1200°C crystallization of high-temperature cristobalite (SiO_2) from a Si-rich amorphous phase takes place. Additionally, in the Si-rich amorphous phase formed at kaolinite-muscovite interfaces, secondary mullite crystallization occurs at ~1300°C. The impurities in the starting kaolin can induce a liquid phase during firing.

Several studies attributed the secondary mullite formation in the kaolinite-alumina mixture to the dissolution of alumina by the silica-rich liquid containing impurities, which form a transitory liquid phase from which mullite nucleated and grew by a "solution-precipitation" mechanism, yet it was reported by authors [12, 14, 25–28, 31, 32, 39, 40] as secondary mullite.

In the present study; the secondary mullite arose from the dissolution of the primary mullite phase in the glassy phase, giving acircular shaped crystals. Meanwhile, the only stoichiometric mullite composition was achieved by the crystallization of metakaolin. The mullite crystallizing out of the liquid phase was rich in silica, as determined by EDS, i.e., Al/Si =2.1, while that resulting from alumina grains was rich in alumina, i.e., Al/Si=5.1. The studied system is a non-equilibrium state. This may be attributed to the fact that the siliceous liquid phase present was not enough to dissolve both the primary mullite and the mullite formed by the diffusion reaction of silica into the alumina grains to recrystallize an acircular secondary mullite with a stoichiometric composition. So the results are three distinct polymorphs of mullite in the fired samples, as identified in the microstructure studied.

4 Conclusion

- The primary mullite crystals preserve the hexagonal platy shape of the original structure of the kaolinite mineral.
- In a kaolinite-alumina system, the microstructure of the formed phases is affected by several parameters, such as temperature; i.e., secondary mullite starts to appear at 1400 °C by the dissolution of the primary one in the glassy phase.
- The secondary mullite formed in such a condition in this study exhibits acircular shaped.

- Mullite bodies processed by uniaxial pressing utilizing 15 wt.% water at 1500 °C for 2 h exhibited the highest compressive strength of 154 MPa and bulk density of 2.1 g/cm3, as well as an open porosity of 35%.
- The formation of the interlocked mullite crystals and grain growth hinder the densification from 1400 to 1500 °C, while the interlocked structure is reasonable for the high mechanical properties of the fired bodies.
- The type and amount of the plasticizer, pressing mode, and sintering temperature can drastically affect the final product properties and, accordingly, their applications.
- The results showed that the porous mullite bodies prepared in the present work could potentially be used to make ceramic filters.

Authors' Contributions All authors contributed to the following:, conception and design of the study, acquisition of data, analysis and/or interpretation of data, Drafting the manuscript, revising the manuscript critically for important intellectual content, Approval of the version of the manuscript to be published.

Amira M. EL-Rafei and T. S. Mansour contributed to the following, Conception and design of the study, acquisition of data, analysis and/or interpretation of data, Drafting the manuscript, revising the manuscript critically for important intellectual content, Approval of the version of the manuscript to be published.

Funding Open access funding provided by The Science, Technology & Innovation Funding Authority (STDF) in cooperation with The Egyptian Knowledge Bank (EKB).

Data Availability Data and materials are all available and prepared, authors will be pleased to provide it if requested during the publication process.

Code Availability Not applicable

Declarations

Consent for Publication All authors approved the version of the manuscript to be published.

Consent to Participate A written informed consent was taken from all participants.

Competing Interests The authors declare no competing interests.

References

1. Rashad M, Balasubramanian M (2018) Characteristics of porous mullite developed from clay and $AlF_3{\cdot}3H_2O$. J Eur Ceram Soc 38(10):3673–3680
2. Zhu Zhiwen, Wei Zhaoling, Sun Wenping, Hou Jie, He Baohui, Dong Yingchao (2016) Cost-effective utilization of mineral-based raw materials for preparation of porous mullite ceramic membranes via in-situ reaction method. Appl Clay Sci 120:135–141
3. Ma Beiyue, Chang Su, Ren Xinming, Gao Zhi, Qian Fan, Yang Wengang, Liu Guoqi, Li Hongxia, Jingkun Yu, Zhu Qiang (2019) Preparation and properties of porous mullite ceramics with high-closed porosity and high strength from fly ash via reaction synthesis process. J Alloys Compd 803(30):981–991
4. Abbasi M, Salahi A, Mirfendereski M, Mohammadi T, Rekabdar F, Hemmati M (2012) Oily wastewater treatment using mullite ceramic membrane. Desalination Water Treatment. 37:21–30
5. Stjernberg J, Lindblom B, Wikstroṁ J, Antti ML, Ode'n M (2010) Microstructural characterization of alkali metal mediated high temperature reactions in mullite based refractories. Ceram Int 36:733–740
6. Dannert C, Durschang B, Raether F (2001) Optimisation of sintering processes for porcelain using in-situ measuring methods. Materials Week 2000, Munich, Germany, Symp. I3 Process Development 1–6
7. Yuan Weiquan, Kuang Jingzhong, Huang Zheyu, Mingming Yu (2022) Effect of aluminum source on the kinetics and mechanism of mullite preparation from kaolinite. Chem Physics Lett 787:139242
8. Martino'n-Torres Marcos, Freestone Ian C, Hunt Alice, Rehren Thilo (2008) Mass-produced mullite crucibles in medieval europe: manufacture and material properties. J Am Ceram Soc 91(6):2071–2074
9. Stjernberg J, Olivas-Ogaz MA, Antti M-L, Ion JC, Lindblom B (2013) Laboratory scale study of the degradation of mullite/corundum refractories by reaction with alkali-doped deposit materials. Ceram Int 39:791–800
10. Schuller KH (1964) Reaction between mullite and glassy phase in porcelain. Trans Br Ceram Soc 63(2):103–17
11. Lopez SYR, Rodriguez JS, Sueyoshi SS (2013) Microstructural characterization of sanitaryware, the relationship spinel and mullite. J Ceram Process Res 14(4):492–497
12. De Aza AH, Turrillas X, Rodriguez MA, Duran T, Pena P (2014) Time-resolved powder neutron diffraction study of the phase transformation sequence of kaolinite to mullite. J Eur Ceram Soc 34:1409–1421
13 Lee WE, Souza GP, Mc Conville CJ, Tarvornpanich T, Iqbal Y (2008) Mullite formation in clays and clay-derived vitreous ceramics. J Eur Ceram Soc 28:465–471
14. Chen G, Qi H, Xing W, Xu N (2008) Direct preparation of macroporous mullite supports for membranes by in situ reaction sintering. J Membrane Sci 318(1):38–44
15. Sainz MA, Serrano FJ, Amigo JM, Bastida J, Caballero A (2000) XRD microstructural analysis of mullites obtained from kaolinite-alumina mixtures. J Eur Ceram Soc 20(4):403–412
16 Rashad M, UmmenSabu G, Logesh MB (2019) Development of porous mullite and mullite-Al_2O_3 composite for microfiltration membrane applications. Sep Purif Technol 219:74–81
17. Garmsiri E, Rasouli Y, Abbasi M, Izadpanah AA (2017) Chemical cleaning of mullite ceramic microfiltration membranes which are fouled during oily wastewater treatment. J Water Process Eng 19:81–95
18. Deutou NJG, Beda T, Biesuz M, Boubakar L, Melo UC, Kamseua E, Sglavo VM (2018) Design and characterization of porous mullite based semi-vitrified ceramics. Ceram Int 44(7):7939–7948
19. Hou Zhaoping, Liu Cheng, Liu Liangliang, Zhang Shaowei (2018) Microstructural evolution and densification behavior of

porous kaolin-based mullite ceramic added with MoO_3. Ceram Int 44(15):17914–17918
20. Hou Zhaoping, Cui Bingxia, Liu Liangliang, Liu Qiang (2016) Effect of the different additives on the fabrication of porous kaolin-based mullite ceramics. Ceram Int 42(15):17254–17258
21. Esharghawi A, Penot C, Nardou F (2009) Contribution to porous mullite synthesis from clays by adding Al and Mg powders. J Eur Ceram Soc 29:31–38
22. Balmori-Ramírez H, Rocha-Rangel E, Refugio-García E, Bradt RC (2004) Dense mullite from attrition-milled kyanite and aluminum metal. J Am Ceram Soc 87:144–146
23. Khabas TA, Nevvonen OV, Vereshchagin VI (2005) Synthesis of mullite in the presence of nanodisperse aluminum powder. Refract Ind Ceram 46:71–75
24. Chen Chin-Yi, Tuan Wei-Hsing (2002) Evolution of mullite texture on firing tape-cast kaolin bodies. J Am Ceram Soc. 85(5):1121–26
25. da Silva VJ, da Silva MF, Gonçalves WP, de Menezes RR, de Araújo Neves G, de Lucena Lira H, de Lima Santana LN (2016) Porous mullite blocks with compositions containing kaolin and alumina waste. Ceram Int 42:15471–15478
26. Chen CY, Lan GS, Tuan WH (2000) Preparation of mullite by the reaction sintering of kaolinite and alumina. J Eur Ceram Soc 20:2519–2525
27. Chen CY, Lan GS, Tuan WH (2000) Microstructural evolution of mullite during the sintering of kaolin powder compacts. Ceram Int 26:715–720
28. Kuo-Chung Liu G, Thomas A, Caballero JS, Moya S. De, Aza, (1994) Mullite formation in kaolinite-α-alumina. Acta Metall Mater 42(2):489–495
29. Behera PS, Bhattacharyya S (2021) Effect of different alumina sources on phase formation and densification of single-phase mullite ceramic–Reference clay alumina system. Mater Today Commun 26(8):101818
30. Ma Jie, Ye Feng, Zhang Biao, Jin Yicheng, Yang Chunping, Ding Junjie, Zhang Haoqian, Liu Qiang (2018) Low-temperature synthesis of highly porous whisker-structured mullite ceramic from kaolin. Ceram Int 44(11):13320–13327
31 Temuujin J, Mac Kenzie KJD, Schmucker M, Schneider H, McManus J, Wimperis S (2000) Phase evolution in mechanically treated mixtures of kaolinite and alumina hydrates (gibbsite and boehmite). J Eur Ceram Soc 20:413–421
32. Chargui Fouzia, Hamidouche Mohamed, Belhouchet Hocine, Jorande Yves, Doufnoune Rachida, Fantozzi Gilbert (2018) Mullite fabrication from natural kaolin and aluminium slag. Boletín de la Sociedad Española de Cerámica y Vidrio 57(4):169–177
33. Gualtieri A, Bellotto M, Artioli G, Clark SM (1995) Kinetic study of the kaolinite-mullite reaction sequence", Part II: Mullite formation. Physics Chem Minerals 22:215–222
34 Chen Y-F, Wang M-C, Hon M (2004) Phase transformation and growth of mullite in kaolin ceramics. J Eur Ceram Soc 24:2389–2397
35. Pongphot Santi, Thiansem Sakdiphon (2016) The effect of alumina (Al_2O_3) on the characteristics of sintered mullite-cordierite Ceramics Synthesized with Kaolin from Naratiwas of Thailand. Key Eng Mater 690:65–70
36. Lee WE, Iqbal Y (2001) Influence of mixing on mullite formation in porcelain. J Eur Ceram Soc 21:2583–2586
37. Tarvornpanich T (2007) Recycled colourless soda-lime-silica glass as an alternative flux in white wares. Ph.D. Thesis. University of Sheffield. https://etheses.whiterose.ac.uk/14505/1/485068.pdf
38. Percival HJ, Duncan JF, Foster PK (1974) Interpretation of the kaolinite-mullite reaction sequence from infrared absorption spectra. J Am Ceram Soc 57(2):57–61
39. Brasileiro MI, Oliveira DHS, Lira HL, Santana LNL, Neves GA, Novaes AP, Sasak JM (2006) Mullite preparation from kaolin residue. Mater Sci Forum 530–531:625–630
40. Viswabaskaran V, Gnanam FD, Balasubramanian M (2004) Mullite from clay–reactive alumina for insulating substrate application. Appl Clay Sci 25:29–35